Modelling the WITT wave energy converter

Sarah Crowley[1], Richard Porter[1],
Dominic Taunton[2] & Philip Wilson[2]
[1]School of Mathematics, University of Bristol, University Walk,
Bristol, BS8 1TW, UK.
[2] Faculty of Engineering and the Environment, University of Southampton,
Lanchester Building, Southampton, SO17 1BJ, UK.

1 Introduction

This presentation describes work undertaken as part of INNOVATE UK funding led by Witt Energy Ltd to investigate the efficacy of a novel design of wave energy converter (WEC). A sealed spherical hull is floating on the surface of the water (Fig. 2(b)) and is moored to the sea bed under a four point catenary mooring system. A mechanical device known as the WITT (Fig. 1) is housed within the hull and generates power via a heavy compound pendulum which is free to pivot independently about either horizontal axis. When waves excite the WITT WEC the motion of the pendulum is transferred into a single unidirectional output from which mechanical energy is converted into electrical energy. The device has some similarities to the SEAREV design and Wello Oy Penguin. There are signficant differences. For example, the mooring design used here is crucial in providing multiple device resonances which result in a broadbanded response in power capture characteristics.

The project includes a number of partners whose combined goal is to estimate the Levelised Cost of Energy (LCOE) of a WITT WEC. The University of Bristol have developed a mathematical model of the operation of the WITT WEC in waves and have used this model to produce a numerically optimised design at different scales in a realistic wave climate and using constraints imposed from practical engineering considerations. The University of Southampton have conducted experimental tank

Figure 1: A photo of a prototype of the WITT pendulum mechanism

testing to validate and test the model assumptions used in the theoretical model.

2 Operation and assumptions

Fig. 3 depicts the configuration of the model of the WITT WEC. The spherical hull is assumed to sit semi-immersed in the undisturbed fluid. A heavy chain four point catenery system is modelled by point masses placed an arbitrary distance along inextensible lines. All mooring parameters, including points of attachment to the hull and the bed are treated as free and their values are determined as part of a constrained

(a) (b)

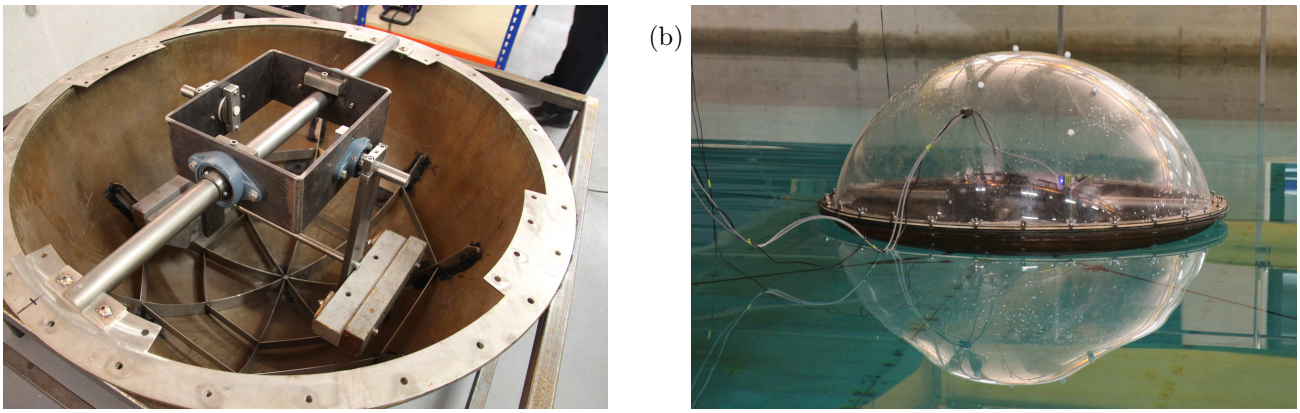

Figure 2: Images of the experimental set up: In (a) the internal set-up of the sphere used in the experimental tests and (b) the sphere semi-submerged during tank-testing.

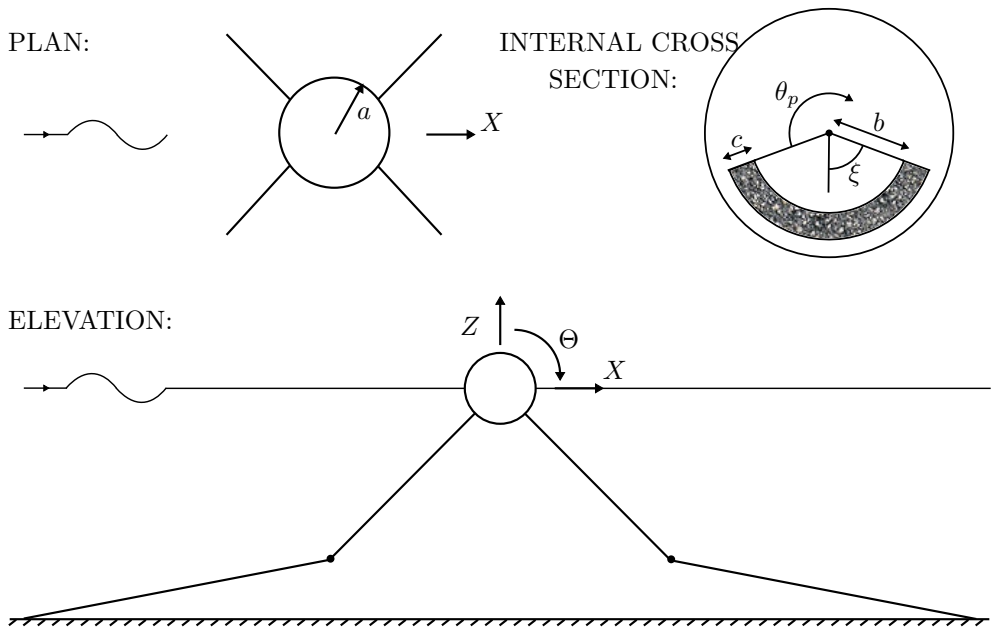

Figure 3: Sketch in plan, elevation and internal cross section of the system

optimisation. The same is true of the parameters which configure the internal pendulum system. For simplicity it is assumed that the pendulum will only move about a single horizontal axis which will be aligned perpendicular to the dominant incident wave direction.

Under the action of incident waves, the hull is allowed to move in surge, heave and pitch ($X(t)$, $Z(t)$, $\Theta(t)$) and the mooring provides restoring forces to each of the motions. The internal pendulum has a motion given by $\theta_p(t)$ and is restored by gravity. Power is taken off via a damper which is assumed to acts in proportion to angle of rotation of the pendulum $\theta_p(t)$ relative to the rotation of the hull $\Theta(t)$. In our model a point mass is positioned on the lower vertical axis of the spherical shell, representing the combined effect of ballast, the WITT gearbox and (Power Take Off) PTO machinery such that the centre of gravity of the hull and the point mass lies some distance below the centre of the sphere. Resolving the vertical forces on the sphere and mooring lines determines the mass of ballast required for the device to be semi-submerged when in equilibrium.

Throughout the modelling a small-amplitude assumption is made so that the linearised theory of water waves can be exploited. For example, the fluid is assumed to be inviscid and incompressible and its motion irrotational. Waves are assumed to be of small steepness and motions of the cylinder and pendulum are assumed to be small in relation to appropriate scales. The effects of turbulent and viscous drag on the motion of the hull are neglected as well as mechanical losses within the PTO.

3 Theoretical modelling

The Euler-Lagrange equations are used to describe the motion of the hull due to hydrodynamic and hydrostatic forces and external forces from the mooring and the PTO. When linearised and after a time harmonic dependence $\mathrm{e}^{-\mathrm{i}\omega t}$ is factorised from the equations, they can be expressed as

$$-\mathrm{i}\omega \mathsf{M}\boldsymbol{U} = \boldsymbol{X}_w - \frac{\mathrm{i}}{\omega}\left(\mathsf{C}+\mathsf{K}\right)\boldsymbol{U} + \boldsymbol{X}_e, \tag{1}$$

where $\boldsymbol{U} = (U_x, U_z, U_\Theta, v)^T$ is the unknown vector of velocties in each of the three hull motions with v representing the relative rotation of the pendulum against the hull. The matrices M, C and K include, respectively, inertia coefficients, and the effects of hydrostatic restoring forces and mooring spring forces. All are determined in terms of the geoemetrical parameters. The vector $\boldsymbol{X}_w = (X_{w,1}, X_{w,2}, 0, 0)^T$ represents the total wave forces in each mode of motion and is decomposed using

$$\boldsymbol{X}_w = \boldsymbol{X}_s(\beta) + (\mathrm{i}\omega\mathsf{A} - \mathsf{B})\boldsymbol{U}, \tag{2}$$

into static wave forces dependent on the incident wave direction β and radiation wave forces characterised in the usual way in terms of frequency dependent added inertia and damping matrices A and B. The effect of the PTO is modelling in (1) by

$$\boldsymbol{X}_e = -\gamma \mathsf{G}\boldsymbol{U}, \tag{3}$$

where γ is the real damping PTO parameter and $\mathsf{G}_{ij} = \delta_{i4}\delta_{j4}$ for $i, j = 1, 2, 3, 4$.

The mean *power* absorbed by the device can be shown, after considerable effort, to be given by

$$W = \frac{1}{4}\frac{\left|X_{s,1}\mathsf{E}_{41} + X_{s,2}\mathsf{E}_{42}\right|^2}{\left|\mathsf{E}_{44}\right|^2\left(|Y| + \mathrm{Re}\{Y\}\right)}\left(1 - \frac{\left(\gamma - |Y|\right)^2}{|\gamma + Y|^2}\right) \tag{4}$$

where

$$Y = \mathsf{Z}_{44} + \left(\mathsf{Z}_{14}\mathsf{E}_{14} + \mathsf{Z}_{24}\mathsf{E}_{24} + \mathsf{Z}_{34}\mathsf{E}_{34}\right)/\mathsf{E}_{44}, \tag{5}$$

$$\mathsf{E} = \left(\mathsf{Z} + \gamma\mathsf{G}\right)^{-1}, \qquad \mathsf{Z} \equiv \mathsf{B} - \mathrm{i}\omega\left(\mathsf{A} + \mathsf{M} - \omega^{-2}(\mathsf{C}+\mathsf{K})\right). \tag{6}$$

The relation (4) has many desirable properties. It can be computed very quickly, a key requirement for numerical optimisation. But we can also see that tuning the PTO to $\gamma = |Y|$ gives the *optimal power*

$$W_{opt} = \frac{1}{4}\frac{\left|X_{s,1}\mathsf{E}_{41} + X_{s,2}\mathsf{E}_{42}\right|^2}{\left|\mathsf{E}_{44}\right|^2\left(|Y| + \mathrm{Re}\{Y\}\right)}. \tag{7}$$

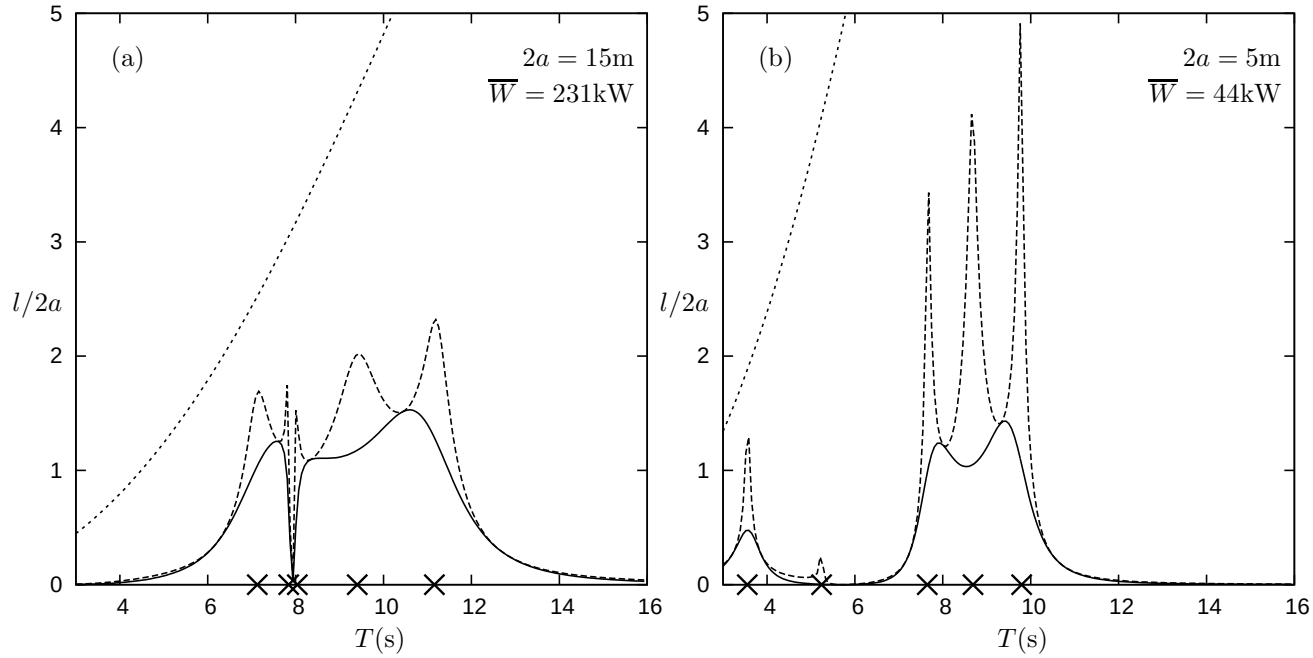

Figure 4: Maximum, optimum and achievable capture width ratio, $l/2a = W/(2aW_{inc})$, for a device of diameter (a) $2a = 15$m and (b) $2a = 5$m, under head seas. The crosses indicate the resonant periods at which $\mathrm{Im}\{Y\}$ vanishes.

and further that it transpires that this has an upper bound

$$W_{opt} \leq \frac{1}{8}\frac{|X_{s,1}E_{41} + X_{s,2}E_{42}|^2}{B_{11}|E_{41}|^2 + B_{22}|E_{42}|^2} < W_{max} \tag{8}$$

with equality when $\mathrm{Im}\{Y\} = 0$ and where $W_{max} = (3\Lambda/2\pi)W_{inc}$ is the theoretical *maximum power*, Λ is the incident wavelength and W_{inc} is the power per unit length of the incident wave. This information allows us both to analyse the resonances of the device and then tune it to operate optimally.

Fig. 4 shows two realisations for a 15m and a 5m sphere of the actual power, W for a fixed γ, the optimal power W_{opt} which can be achieved when γ is allowed to vary with frequency ω and W_{max} the (unattainable, due to (8)) maximum theoretical power. Also shown using crosses are values where $\mathrm{Im}\{Y\} = 0$ where the device is resonant. Thus we see there are as many as five resonances across a broad range of periods for an optimised WEC. A numerical optimisation distributes these to maximise the power harnessed by the WITT WEC and values of mean power $\overline{W}$ for each size of device under the EMEC wave climate are also displayed in Fig. 4.

4 Experimental validation

Fig. 5 show the device RAOs following wave tank testing at Plymouth University of a 1.2m diameter sphere fitted with a model pendulum (see Fig. 2(a)) without a PTO

attached. Elastic bungee cord lines were used for these experiments and the theory was modified accordingly to incorporate these effects in K. Ballast was used to weigh down the sphere to nearly half submergence although the lip on the sphere caused some difficulties with slamming loads in motion. Except for the Fig. 5(d) – which we suspect is due to contanimated data – the agreement between theory and experiment seems very good even for the steepest waves.

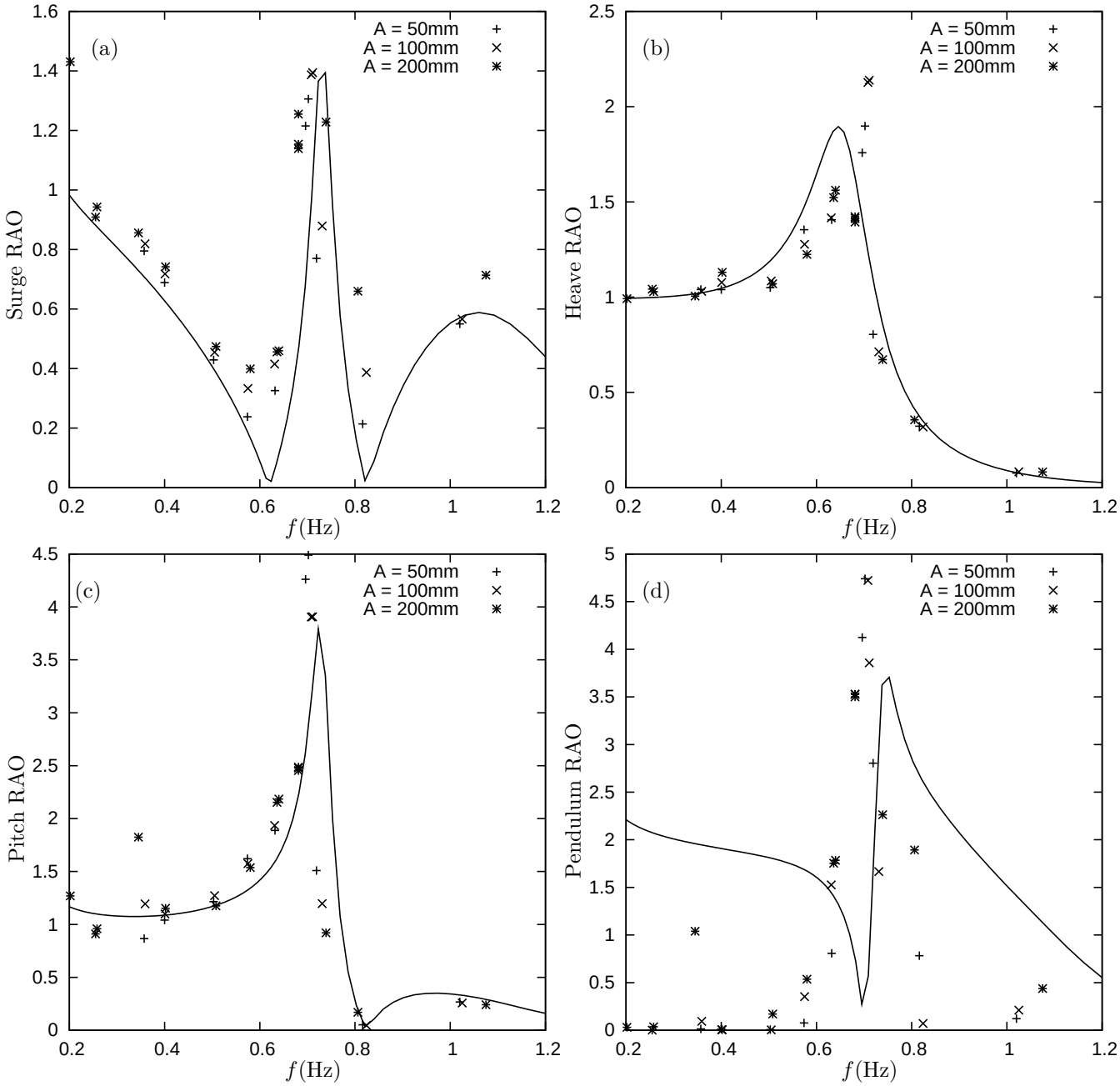

Figure 5: Comparison of the theoretical (line) and experimental (points) results. In (a) the surge; (b) heave; (c) pitch and (d) relative pendulum RAOs are plotted. The different symbols represent results from different incident wave heights used in the experiments.

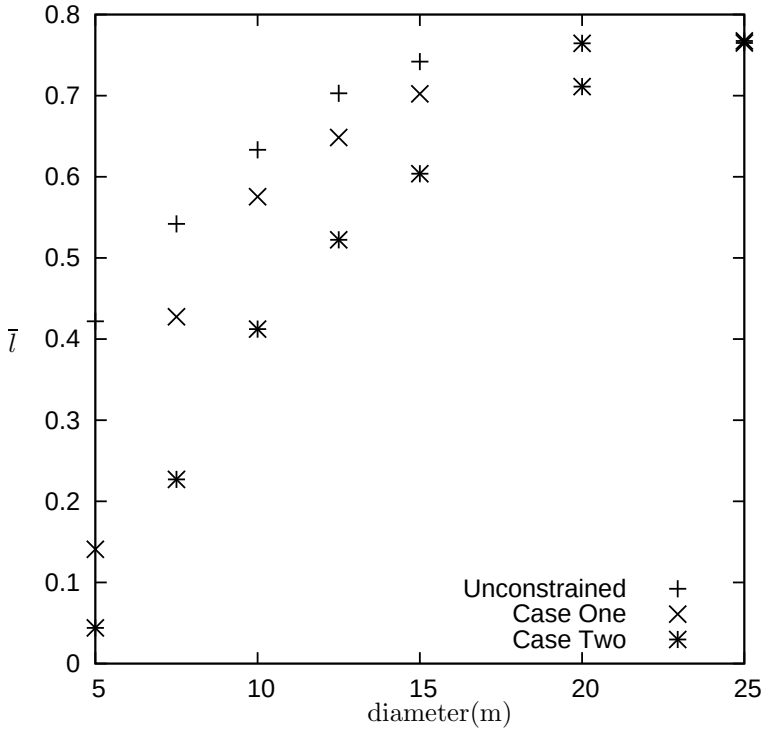

Figure 6: Mean capture factor against device size and the effect of motion constraints.

5 Optimisation

Most of the results are based on a dimensionless *mean* capture factor

$$\bar{l} = \frac{\overline{W}}{\overline{W}_{inc} 2a}, \tag{9}$$

which uses the power weighted over a model wave energy density spectrum $\tilde{S}(T, \beta)$

$$\overline{W} = \rho g \int_{-\pi}^{\pi} \int_{0}^{\infty} c_g(T) \tilde{S}(T, \beta) l(T, \beta) T^{-2} \, \mathrm{d}T \, \mathrm{d}\beta, \qquad \text{where} \quad l(T, \beta) = \frac{W}{W_{inc}}, \tag{10}$$

is the capture width of the device expressed in terms of period T and angle of incidence β. $\overline{W}_{inc}$ is the equivalent mean incident wave energy per unit length and c_g is the group velocity.

Results of applying a numerical optimisation over different sized cylinder and under three different levels of motion constraint are summarised in Fig. 6. The wave energy data from the EMEC site in Scotland is used to generate the wave energy density spectrum. In Case One, the relative motion of the pendulum is constrained to 60° and the surge motion to one hull diameter (per 2m wave height). In Case Two the values of these constraints are halved. Unconstrained motions can lead to results which invalidate the underlying model assumptions.

A good insight into the optimisation of the device size can gained by comparing the capture factor normalised against surface area and mass and the result of performing

	Case One			Case Two		
Hull diam. (m)	$\bar{l}$	$\bar{l}_s$	$\bar{l}_m$	$\bar{l}$	$\bar{l}_s$	$\bar{l}_m$
5	0.14	3.27	4.91	0.04	1.02	1.37
7.5	0.43	6.42	**6.66**	0.23	3.51	3.37
10	0.58	**6.67**	5.34	0.41	4.78	**3.59**
12.5	0.65	5.98	3.77	0.52	**4.85**	2.98
15	0.70	5.35	2.75	0.60	4.67	2.41

Table 1: Absorbed energy per submerged surface area $\bar{l}_s$ (Mwh/m^2) and absorbed energy per total device mass $\bar{l}_m$ (Mwh/t).

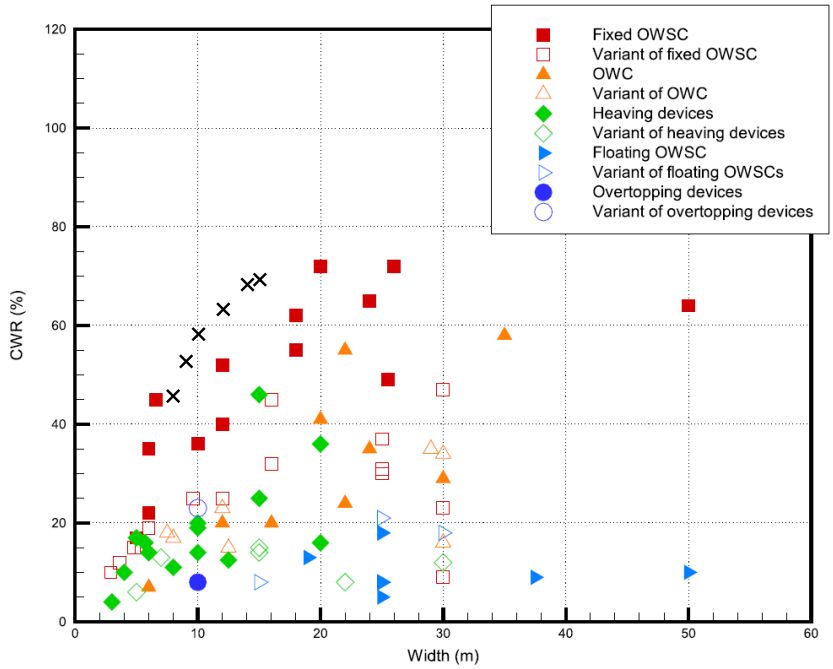

Figure 7: Mean capture factor against device width. The overlaid black crosses represent the results for the WITT WEC given in Table 1 for Case One.

these calculations for different hull sizes is summarised in Table 1 which suggests a device about 10m in diameter is optimal. The results from Case One in Table 1 for the WITT WEC is compared with data from Babarit (2015, Renewable Energy **80** 610–628) across a variety of existing WECs and appears to compare very well.

Acknowledgements

The authors would like to acknowledge funding from EPSRC (EP/N508640/1 and EP/N508652/1). The authors are also grateful to Witt Energy Limited and other project partners of the INNOVATE UK consortium for direction on this project.